JOURNAL OF SPACECRAFT AND ROCKETS
Vol. 43, No. 5, September–October 2006

Preliminary Design of Low-Thrust Multiple Gravity-Assist Trajectories

P. De Pascale*
University of Padova, 35131 Padova, Italy
and
M. Vasile†
Politecnico di Milano, 20156 Milan, Italy

DOI: 10.2514/1.19646

The availability of electric engines as primary sources of propulsion has opened the doors to new scenarios for future interplanetary missions, but has increased the complexity of trajectory design. This paper proposes a novel approach to the preliminary design of interplanetary trajectories characterized by a combination of low-thrust propulsion and multiple gravity-assist maneuvers. Low-thrust arcs are obtained by shaping the trajectory through a set of parameterized pseudoequinoctial elements. The characterization of the solution space for a particular set of planetary encounters and a range of launch dates is then performed through a global optimization method, blending a particular evolutionary algorithm with a deterministic domain decomposition technique. The effectiveness of the proposed approach is demonstrated through a number of examples of the design of low-thrust, gravity-assist interplanetary trajectories.

Nomenclature

F	=	objective function
f_p	=	augmented objective function
L	=	true longitude, rad
m_0	=	spacecraft initial mass, kg
m_p	=	propellant mass, kg
m_r	=	propellant mass ratio
N_P	=	number of planets
n_R	=	number of revolutions
$\boldsymbol{r}$	=	position vector, km
$\ddot{\boldsymbol{r}}$	=	acceleration vector, km/s^2
r_p	=	ratio between the flyby radius and the planet radius
T	=	time of flight, day
$\boldsymbol{u}$	=	thrust acceleration vector, m/s^2
$\boldsymbol{v}$	=	velocity vector, km/s
v	=	true anomaly, rad
$\tilde{\mathbf{v}}_i$	=	flyby incoming relative velocity, km/s
$\tilde{\mathbf{v}}_o$	=	flyby outgoing relative velocity, km/s
v_∞	=	hyperbolic excess velocity, km/s
$\boldsymbol{y}$	=	state vector
$\boldsymbol{\alpha}$	=	orbital elements
$\tilde{\boldsymbol{\alpha}}$	=	pseudoequinoctial elements
ε	=	percentage of time of the deep-space maneuver or switching time
θ	=	right ascension, rad
$\boldsymbol{\lambda}$	=	shaping parameter vector
μ	=	gravitational parameter of the central body, km^{3}s^{-2}
φ	=	phase parameter, rad
ψ	=	declination, rad
Ω	=	longitude of the ascending node, rad
ω	=	argument of perihelion, rad
Δv	=	variation of velocity, km/s

Superscript

(k)	=	value of a variable related to phase kth

Received 23 August 2005; revision received 1 March 2006; accepted for publication 8 March 2006.

*Ph.D. Candidate, Center of Studies and Activity for Space, Via Venezia 15. Member AIAA.
†Assistant Professor, Department of Aerospace Engineering, Via La Masa 34. Member AIAA.

I. Introduction

NASA's Deep Space 1 [1] and recently ESA's SMART-1 [2] have shown the effectiveness of low-thrust systems as primary propulsion devices [3]. This form of propulsion opens the door to new kinds of missions in the solar system [4,5], exploiting the beneficial effects given by the combination of gravity-assist maneuvers and low thrust. In recent studies, missions to Mercury [6–8], Jupiter [9–11], and the sun [12] have been designed, resorting to a combination of low-thrust and multiple swingbys [13]. Such new scenarios, characterized by new propulsion systems and by highly challenging mission objectives, make the task of mission analysts more difficult than ever. In fact, the design of low-thrust transfers generally requires the solution of an optimal control problem [14,15], which has no general solution in closed form.

Although many different methods have been developed to tackle these trajectory design problems, it is common practice [16] to classify them into two large families: direct [17,18] and indirect methods [19,20]. The former family contains all of those methods that transcribe the infinite dimension optimal control problem into a finite parameter optimization problem and then solve the resulting system of nonlinear algebraic equations with a general nonlinear programming approach [14]. Several flavors of transcription methods have been devised [21,22] including shooting techniques, collocation methods based on the Hermit–Simpson formula [23], Lobatto quadrature [24], finite elements in time [22] or multispectral methods, and differential inclusion [25]. The latter family collects all of those methods that explicitly derive the necessary conditions for optimality [26] as given by the optimal control theory. The solution of the resulting differential algebraic system of equations with boundary conditions is then performed through numerical integration and some kind of gradient method. It is worth mentioning, in the latter class, the gradient-restoration approach of Miele and Wang [27]. More recently, the application of the dynamic programming principles have produced quite interesting results even in very complex cases [28].

All of these approaches need to be initialized with a first-guess solution that, depending on the particular method, can either be quite far from the final optimal solution or needs to be very close to it. The

generation of a suitable first guess turns out to be a tricky and quite time-consuming task because it deeply affects the final result as well as the convergence of all the aforementioned methods. For this reason, all of the preceding approaches are unsuitable for the preliminary assessment of a large number of solutions, such as those usually required in conceptual studies.

The main difficulty is due to the unavailability of sufficiently general analytical solutions; in fact, few cases of analytical solutions of a thrusting spacecraft exist in literature [29,30] and, although very interesting, they are quite specialized (i.e., only two-dimensional or useful only for particular trajectories). For more general cases, numerical propagation is necessary, with a consequentially considerable computational effort even in a very preliminary phase.

Studies on the characterization of transfer options for low-thrust trajectories and on the generation of first-guess solutions date back to the late nineties with the works of Hartmann et al. [31], where multiobjective genetic algorithms were first used to compute first-guess solutions for an indirect method. The derivation of an approximate analytical solution was addressed in the works of Markopoulos [30], Azimov and Bishop [32,33]. The former has provided a sort of generalization of non-Keplerian analytical solutions for the case of a thrusting spacecraft, whereas the latter two have directly tackled the solution of the optimal control problem for a low-thrust trajectory with very interesting results.

Inspired by the work of Tanguay [34], Petropoulos et al. [35], Petropoulos [36], and Petropoulos and Longuski [37] proposed a shape-based approach that represents the trajectory (connecting two points in space) with a particular parameterized analytical curve (or shape) and computes the control thrust necessary to satisfy the dynamics. Although the resulting trajectory is not the actual solution of an optimal control problem, by tuning the shaping parameters it is possible to generate solutions sufficiently good to feed into a finer optimization process.

More precisely, in the work by Petropoulos [36], a thrust arc is represented by an analytical curve, known as exponential sinusoid, which is determined by five free shape parameters in polar coordinates. This shape is suitable for the approximation of planar motion. However, due to the reduced number of shaping parameters, the boundary conditions on position and velocity cannot be solved simultaneously to satisfying the constraints on the time of flight (TOF) and on the level of acceleration. For three-dimensional (3-D) problems, the propellant consumption for out-of-plane motion is only estimated [35].

The goal of this paper is to contribute to the field of research on preliminary design methodologies by providing an approach that overcomes some of the limits of previous methods. More precisely, the aim is to address the fast and extensive characterization of the solution domain for low-thrust multiple gravity-assist trajectories (LTGA). This characterization is achieved through the combination of a novel shape-based approach for the solution of low-thrust arcs with an innovative global optimization technique [38]. The method developed in this work is based on the description of the evolution of the trajectory through a set of pseudoequinoctial elements. This approach allows for a full 3-D representation of LTGA trajectories with an implicit satisfaction of boundary conditions on states. In addition, it will be shown how the proposed shapes, though requiring a limited number of free parameters, are extremely flexible at representing different optimal control profiles. The effectiveness of the proposed approach is demonstrated through different trajectory design problems of increasing difficulty.

II. Low-Thrust Gravity-Assist Trajectory Modeling

A. Inverse Method

Considering a given proper set of solutions for a trajectory connecting two points in a central force field, it is always possible to obtain, through algebraic computation, the necessary acceleration of a propulsive system by

$$\boldsymbol{u} = \ddot{\boldsymbol{r}} + \mu \frac{\boldsymbol{r}}{r^3} \tag{1}$$

where $\boldsymbol{r}$ is in a Cartesian reference frame. However, Cartesian parameters (position and velocity) have a large variation with time, even for a simple circular orbit. Representing their time evolution with a good level of accuracy by means of a general polynomial expansion, like in collocation methods [17,22–24], would require a high-order polynomial (or, equivalently, a considerable number of collocation points) even for a single revolution of an unperturbed orbit. On the other hand, the time evolution of Cartesian parameters for an unperturbed circular orbit can be expressed by means of Keplerian parameters as a simple trigonometric function of time.

In general, an efficient and accurate description of the evolution of the trajectory under the effect of a low-thrust action can be obtained by means of orbital elements; in fact, the solution of the perturbed two-body problem in terms of these elements can be generally written in the form

$$\alpha_i(t) = \alpha_{0i} + \delta\alpha_i(t) \tag{2}$$

where α_0 is the initial condition of the ith parameter, which remains constant if the motion is purely Keplerian, and $\delta\alpha(t)$ is a time-dependent function due to the effects of any perturbative action. The low level of thrust provided by electric engines allows us to consider the propulsive action as a perturbation of the Keplerian motion. Moreover, if the use of thrust has to be minimized, the second term on the right-hand side of Eq. (2) should tend toward zero. If orbital elements are taken instead of Cartesian coordinates, the equations governing the motion of a point mass are [13,23]

$$\dot{\boldsymbol{\alpha}} = \mathbf{A}(\boldsymbol{\alpha})\Delta + \mathbf{b} \tag{3}$$

with $\boldsymbol{\alpha}^T = [p, f, g, h, k, L]$ being the nonsingular modified equinoctial orbital elements defined as follows with respect to the Keplerian orbital elements:

$$p = a(1-e^2), \qquad f = e\cos(\omega+\Omega), \qquad g = e\sin(\omega+\Omega),$$
$$h = \tan(i/2)\cos\Omega, \qquad k = \tan(i/2)\sin\Omega, \qquad L = \nu+\omega+\Omega \tag{4}$$

where a is the semimajor axis, and e and i are, respectively, the eccentricity and the inclination. The second term on the right-hand side of Eq. (3) is

$$\mathbf{b}^T = [0 \quad 0 \quad 0 \quad 0 \quad 0 \quad \sqrt{\mu p}(q/p)^2]$$

and the matrix $\mathbf{A}(\boldsymbol{\alpha})$ is

$$\mathbf{A} = \begin{bmatrix} 0 & 2p/q\sqrt{(p/\mu)} & 0 \\ \sqrt{(p/\mu)}\sin L & \sqrt{(p/\mu)}(1/q)\{(q+1)\cos L + f\} & -\sqrt{(p/\mu)}(g/q)\{h\sin L - k\cos L\} \\ -\sqrt{(p/\mu)}\cos L & \sqrt{(p/\mu)}(1/q)\{(q+1)\sin L + g\} & \sqrt{(p/\mu)}(f/q)\{h\sin L - k\cos L\} \\ 0 & 0 & \sqrt{(p/\mu)}(s^2\cos L)/2q \\ 0 & 0 & \sqrt{(p/\mu)}(s^2\sin L)/2q \\ 0 & 0 & \sqrt{(p/\mu)}(1/q)\{h\sin L - k\cos L\} \end{bmatrix} \tag{5}$$

where $q = 1 + f\cos L + g\sin L$, $s^2 = 1 + h^2 + k^2$, and $\mathbf{\Delta} = [u_r, u_\theta, u_h]^T$ represents the three components of the propulsive acceleration along the radial, transversal, and binormal directions of a rotating coordinate frame centered on the spacecraft. In this work, only propulsive disturbances are considered and equinoctial modified nonsingular elements are adopted to allow the most general representation of either circular, parabolic, or zero inclination orbits.

Because low-thrust trajectories typically require continuous thrust over a large number of revolutions, time can be substituted with the more convenient angular variable $L = \Omega + \omega + \upsilon$, called true longitude. By dividing all of the terms in Eq. (3) by $\mathrm{d}L/\mathrm{d}t = \sqrt{\mu p}(q/p)^2$ and neglecting the perturbing terms, we obtain

$$\bar{\boldsymbol{\alpha}}' = \bar{\mathbf{A}}(\bar{\boldsymbol{\alpha}})\mathbf{\Delta} \tag{6}$$

with $\bar{\boldsymbol{\alpha}}^T = [p, f, g, h, k]$ and $\bar{\mathbf{A}}(\bar{\boldsymbol{\alpha}})$ being the new $[5 \times 1]$ state vector and the new reduced matrix, respectively, and the prime notation indicates derivative with respect to the angular variable L. By assigning a proper functional form $\bar{\alpha}_\iota = E_\iota(L)$ for $i = 1, \ldots, 5$ to the ith equinoctial element $\bar{\alpha}_i$ and computing analytically $\bar{\alpha}_i'(L) = dE_i(L)/dL$, it would be possible to obtain a solution by a least square minimization finding $\mathbf{\Delta}^*$ so that

$$\Phi(\mathbf{\Delta}^*) \equiv \|\bar{\mathbf{A}}\mathbf{\Delta}^* - \bar{\boldsymbol{\alpha}}'\|_2^2 \leq \min_{\mathbf{\Delta}\Re^n}\|\bar{\mathbf{A}}\mathbf{\Delta} - \bar{\boldsymbol{\alpha}}'\|_2^2$$

because the resulting system is overdetermined. This approach turns out to be quite inaccurate at providing acceleration profiles that, when propagated forward, yield relevant errors in terms of terminal position and velocity. A better result could be achieved by solving a multiobjective optimization problem that minimizes both the desired characteristics of the trajectory and the residual of the least square solution.

A more convenient approach is to use equinoctial elements to describe the evolution of the Cartesian coordinates. The transcription of the trajectory in Cartesian coordinates allows for the derivation of the control vector directly from Eq. (1). In fact, the evolution of the Cartesian position vector $\boldsymbol{r}$ can be expressed as a function of the equinoctial elements through the following equation:

$$\boldsymbol{r} = \begin{bmatrix} [r/(1+h^2+k^2)](\cos L + (h^2-k^2)\cos L + 2hk\sin L \\ [r/(1+h^2+k^2)][\sin L - (h^2-k^2)\sin L + 2hk\cos L] \\ [2r/(1+h^2+k^2)](h\sin L - k\cos L) \end{bmatrix} \tag{7}$$

The actual velocity $\boldsymbol{v}$ and acceleration $\ddot{\boldsymbol{r}}$ can be computed by an analytical differentiation of the position vector represented in Eq. (7):

$$\begin{aligned} \boldsymbol{v} &= \mathrm{d}\boldsymbol{r}/\mathrm{d}t = (\mathrm{d}\boldsymbol{r}/\mathrm{d}L)(\mathrm{d}L/\mathrm{d}t), \\ \ddot{\boldsymbol{r}} &= \mathrm{d}\boldsymbol{v}/\mathrm{d}t = (\mathrm{d}\boldsymbol{v}/\mathrm{d}L)(\mathrm{d}L/\mathrm{d}t) \end{aligned} \tag{8}$$

and for the jth component of the position vector $\boldsymbol{r}$ and velocity vector $\boldsymbol{v}$, the derivatives are given by

$$\frac{\mathrm{d}r_j}{\mathrm{d}L} = \sum_{i=1}^{5}\frac{\partial r_j}{\partial\bar{\alpha}_i}\frac{\partial\bar{\alpha}_i}{\partial L} + \frac{\partial r_j}{\partial L}, \qquad \frac{\mathrm{d}v_j}{\mathrm{d}L} = \sum_{i=1}^{5}\frac{\partial v_j}{\partial\bar{\alpha}_i}\frac{\partial\bar{\alpha}_i}{\partial L} + \frac{\partial v_j}{\partial L} \tag{9}$$

with $j = 1, \ldots, 3$. The control acceleration is algebraically obtained from Eq. (1), whereas the propellant mass ratio can be easily computed with the following expression:

$$\frac{m_p}{m_{\mathrm{tot}}} = 1 - \exp\left[-\int_{L_0}^{L_f}\frac{|\boldsymbol{u}|}{I_{\mathrm{sp}}g_0}\frac{\mathrm{d}t}{\mathrm{d}L}\,\mathrm{d}L\right] \tag{10}$$

where m_{tot} is the total initial mass of the spacecraft; L_o and L_f are, respectively, the initial and final true longitude over which the integral is evaluated; I_{sp} is the specific impulse; and $g_0 = 9.81\ \mathrm{m/s^2}$ is the gravitation acceleration at sea level. Additionally, the following time constraint must be respected:

$$T = \int_{L_0}^{L_f}\frac{\mathrm{d}t}{\mathrm{d}L}\,\mathrm{d}L \tag{11}$$

This approach is quite fast and computationally inexpensive, because no propagation is required and the differential problem is reduced to an algebraic one with the additional evaluation of the two quadratures in Eqs. (10) and (11), which are here computed with a tenth-order Gauss–Legendre approximation. Notice that, unlike direct-collocation methods or differential-inclusion-based approaches [25], the trajectory is not discretized and Eq. (1) holds true for every possible time evolution of the position vector $\boldsymbol{r}$. Therefore, no system of nonlinear algebraic equations, either containing the controls or simply the states (as in differential inclusion formulations), needs to be solved to satisfy the dynamic equations. Furthermore, the only constraint that needs to be satisfied to make the solution physical is given by Eq. (11). On the other hand, constraints on controls are explicitly imposed on the value of $\boldsymbol{u}$ obtained by Eq. (1).

B. Shape of the Trajectory

The inverse method described previously requires the definition of the shape of a low-thrust trajectory connecting two points in space. It is therefore fundamental to define the proper family of parameterized curves describing, in terms of equinoctial elements, a low-thrust orbit. As the general evolution of an orbital element can be expressed by Eq. (2), with $\delta\boldsymbol{\alpha}(t)$ being the disturbing effect, the general shape of the equinoctial elements can be approximated as

$$\tilde{\alpha}_i = \tilde{\alpha}_{0i} + E_i(L, \boldsymbol{\lambda}) \tag{12}$$

where the vector $\boldsymbol{\lambda}$ contains a set of shaping parameters that are constant along the whole trajectory, and $\tilde{\alpha}_{0i}$ is the value of $\tilde{\alpha}_i$ for $L = L_0$. The elements $\tilde{\boldsymbol{\alpha}}$ are called pseudoequinoctial elements because they do not always exactly satisfy Gauss' planetary equations unless the thrust is equal to zero. Notice that the value of the shaping parameters is independent of L, therefore the value is constant along the whole thrust arc.

To obtain a set of pseudoequinoctial elements that exactly satisfy the boundary conditions, it is necessary to solve the following sixth-order algebraic system of nonlinear equations:

$$\boldsymbol{v}[\tilde{\boldsymbol{\alpha}}(L_0), L_0] = \boldsymbol{v}_0, \qquad \boldsymbol{v}[\tilde{\boldsymbol{\alpha}}(L_f), L_f] = \boldsymbol{v}_f \tag{13}$$

However, for low values of the propulsive acceleration, as in the case of low-thrust engines, it is often sufficient to solve the easier, linear programming problem for the boundary conditions of the pseudoelements:

$$\tilde{\boldsymbol{\alpha}}(L_0) = \boldsymbol{\alpha}_0, \qquad \tilde{\boldsymbol{\alpha}}(L_f) = \boldsymbol{\alpha}_f \tag{14}$$

The solution of Eq. (14) implies the satisfaction of the boundary constraints on position

$$\boldsymbol{r}[\tilde{\boldsymbol{\alpha}}(L_0), L_0] = \boldsymbol{r}_0, \qquad \boldsymbol{r}[\tilde{\boldsymbol{\alpha}}(L_f), L_f] = \boldsymbol{r}_f \tag{15}$$

but gives just an approximation of the satisfaction of the boundary constraints on the velocity vector. For a more accurate trajectory description, the solution obtained by Eq. (14) is used as a first guess to exactly solve Eq. (13). Because the value of the velocity and position at the boundaries of the transfer leg is a function of the pseudoequinoctial elements and therefore of the shaping parameters, the optimal value of $\boldsymbol{\lambda}$ depends on the values of $\boldsymbol{r}$ and $\boldsymbol{v}$ at the boundaries. In particular, we can expect that, given two points in space and the transfer time, the optimal value for $\boldsymbol{\lambda}$ would correspond to a trajectory that closely matches the corresponding ballistic arc (or Lambert arc) and would satisfy Eqs. (9) and (11).

The analogy with the variation of parameters in the evolution of perturbed orbits may suggest that the effect of a low thrust can be treated as a general perturbation in terms of secular and periodical components, the latter typically having a null net effect averaged over the orbital period. This consideration has led to the following

particular shape (called a linear-trigonometric shape in the following equation):

$$\tilde{\boldsymbol{\alpha}} = \tilde{\boldsymbol{\alpha}}_0 + \tilde{\boldsymbol{\alpha}}_1(L - L_0) + \boldsymbol{\lambda}\sin(L - L_0 + \varphi) \tag{16}$$

where $\boldsymbol{\lambda} = [\lambda_1, \lambda_2, \lambda_3]^T$ is the set of shaping parameters, whereas the values of $\tilde{\boldsymbol{\alpha}}_0$ and $\tilde{\boldsymbol{\alpha}}_1$ depend on the initial and final conditions in Eqs. (13) and (15). The shape presented in Eq. (16) can be seen as a first-order expansion of the evolution of the equinoctial elements, obtained by considering the first-order term of a Taylor series and the first-order term of a Fourier series with unit frequency. In the following expression, λ_1 will be associated to p, λ_2 to the parameters f and g, and λ_3 to the parameters h and k. The additional phase parameter φ was empirically set for each pseudoelement after the analysis of several numerical simulations.

The numerical integration of a tangential thrust law, decreasing with the square of the distance from the sun, shows (see Figs. 1a and 1b) for parameters f and g a typical evolution that is easily approximated by the sum of a linear and a sinusoidal term of the following kind:

$$\begin{aligned} \tilde{f} &= \tilde{f}_0 + \tilde{f}_1(L - L_0) + \lambda_2 \sin(L), \\ \tilde{g} &= \tilde{g}_0 + \tilde{g}_1(L - L_0) + \lambda_2 \cos(L) \end{aligned} \tag{17}$$

The tangential steering law was selected for two reasons: it maximizes the variation of energy of the orbit and is typically used for the generation of first-guess solutions for spiral trajectories. However, as it will be shown in the following discussion, the shapes presented are actually able to accommodate more flexible control profiles.

Figure 1 shows a comparison between the shaped elements $\tilde{f}$ and $\tilde{g}$ and the evolution of the osculating equinoctial elements propagated with a tangential acceleration with a nominal value $u_t = 10^{-4}$ m/s^2. Notice that by manually tuning the value of the shaping parameter λ_2, it was always possible to approximate the evolution of the equinoctial elements as it is shown in Fig. 1, where the value of λ_2 is equally spaced in ten intervals between $\lambda_2 = [-0.03, 0.03]$.

This comparison has been performed for different initial conditions and thrust levels. The resultant adopted shape was found to properly approximate the propagated elements in all cases. An analogous consideration holds true for the evolution of the equinoctial elements h and k, which represent the out-of-plane motion:

$$\begin{aligned} \tilde{h} &= \tilde{h}_0 + \tilde{h}_1(L - L_0) + \lambda_3 \sin(L), \\ \tilde{k} &= \tilde{k}_0 + \tilde{k}_1(L - L_0) + \lambda_3 \cos(L) \end{aligned} \tag{18}$$

The semilatus rectum, instead, can be approximated with a shape of the following kind, as can be seen in Fig. 2a:

$$\tilde{p} = \tilde{p}_0 + \tilde{p}_1(L - L_0) + \lambda_1 \sin(L - L_0) \tag{19}$$

Notice that the average trend of the parameter p in Fig. 2a is actually linear, confirming the hypotheses at the basis of this kind of shape. The shape in Eq. (16) is suitable to approximate the evolution of the equinoctial elements under a thrust that is decreasing with the square

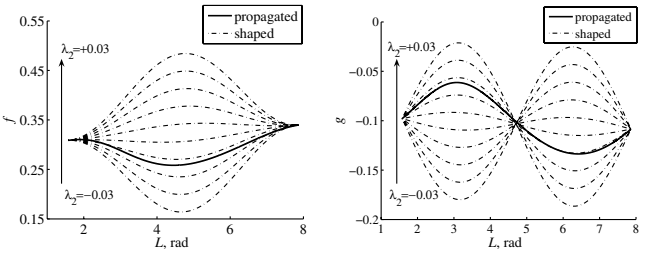

Fig. 1 Effect of the shaping parameter λ_2: a) f element and b) g element.

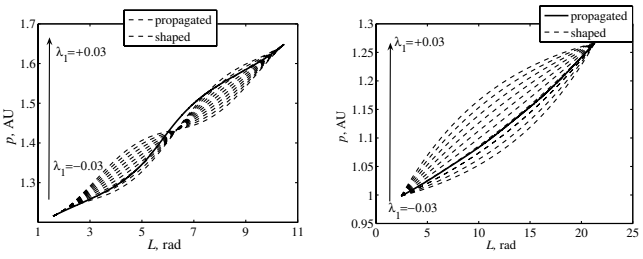

Fig. 2 Effect of the shaping parameter λ_1 on p: a) linear-trigonometric shape and b) exponential shape.

of the distance from the sun, as is the case of solar electric propulsion (SEP). In the case of a constant thrust modulus, as is typical of nuclear electric propulsion systems (NEP), a different shape would be required.

A numerical analysis of the evolution of the equinoctial parameters under the effect of a tangential acceleration with constant modulus, suggests an exponential trigonometric shape of this kind

$$\tilde{\boldsymbol{\alpha}} = \tilde{\boldsymbol{\alpha}}_0 + \tilde{\boldsymbol{\alpha}}_1 e^{\boldsymbol{\lambda}(L-L_0)} \sin[\omega(L - L_0) + \varphi] \tag{20}$$

In this case, the frequency ω and the phase φ are zero for the orbital parameter p, ω is common to all other orbital elements, and the shaping parameters are $\boldsymbol{\lambda} = [\lambda_1, \lambda_2, \lambda_3]^T$. However, it was empirically found that the value of ω, which defines the frequency of the periodical effect, is typically close to zero. This observation motivated a simplification of this shape, dropping the trigonometric part and considering only the mean evolution of the elements:

$$\tilde{\boldsymbol{\alpha}} = \tilde{\boldsymbol{\alpha}}_0 + \tilde{\boldsymbol{\alpha}}_1 e^{\boldsymbol{\lambda}(L-L_0)} \tag{21}$$

By this choice, the description of the periodical term of the evolution of the equinoctial parameters is lost and only the secular effects are considered; however, as it will be shown later, this approximation is sufficient to capture the most relevant characteristics of a general low-thrust transfer with a reduced number of optimization parameters. In general, we can argue that three shaping parameters are the minimum necessary set to control the orbit energy, its in-plane orbit geometry, and the position of the orbit plane in space. Moreover, compared with the linear-trigonometric shape, see Fig. 2a, the exponential shape offers a better flexibility at approximating the mean evolution of the equinoctial-element semilatus rectum p, see Fig. 2b. The exponents $\boldsymbol{\lambda}$ define the curvature and the convexity of the evolution of the shaped elements, setting the speed of growth of the mean parameters and, therefore, the variation of the control profile. It is interesting to underline that, apart from the particular shape, two free constants for each pseudoelement $\tilde{\alpha}_i$, namely $\tilde{\alpha}_{0i}$ and $\tilde{\alpha}_{1i}$, satisfy the boundary conditions of Eq. (14), and the remaining free parameters $\boldsymbol{\lambda}$ properly shape each element in order to meet the requirements and constraints on the thrust profile.

C. Composition of the Trajectory

A full trajectory made of low-thrust coast arcs and multiple swingbys is composed by patching conic arcs and shaped arcs together. For a sequence of N_P planets, the problem is divided into k phases, with $k = 1, \ldots, N_P - 1$. For each phase k, the sequence of coast arcs and thrust arcs is then fixed a priori: depending on the trajectory under study, each phase can be characterized by a pure thrust arc, a thrust-coast arc, a coast-thrust arc, or a pure coast arc with a deep-space maneuver. Therefore, two points in space can be connected either by a conic arc (solution of Lambert's algorithm) or by a low-thrust arc (solution of the proposed inverse method), which represents a sort of extension of Lambert's algorithm.

The relative escape velocity is defined as follows:

$$\boldsymbol{v}_\infty^E = \sqrt{C_3}[\sin\psi\cos\vartheta, \sin\psi\sin\theta, \cos\psi]^T \tag{22}$$

and the relative incoming velocity to each planet, a free parameter, is defined as

$$\tilde{\boldsymbol{v}}_i^{P_i} = [\tilde{v}_{\text{in},x}^{P_i}, \tilde{v}_{\text{in},y}^{P_i}, \tilde{v}_{\text{in},z}^{P_i}]^T \tag{23}$$

whereas the relative outgoing velocity from each flyby is computed with a 3-D linked-conic model [37]. The initial and final conditions for each phase k can be derived from the ephemeris at time t_i for $i = 1, \ldots, N_P$. The procedure is then iterated for all of the defined thrust phases.

In addition, in order to allow the spacecraft to spiral around the sun as many times as necessary, before encountering each planet, an integer auxiliary variable n_R is introduced, representing the number of required revolutions. Therefore, the final true longitude, which defines the final angular position, is modified through

$$\tilde{L}_f = L_f + 2\pi n_R, \qquad n_R = 0, 1, \ldots, n_{\max} \tag{24}$$

Finally, the inverse method is applied to each thrust phase k to obtain the control acceleration vector. Shaping functions for each pseudoorbital parameter are inserted into Eq. (7) and then substituted into Eq. (1) to yield

$$\boldsymbol{u}^{(k)} = \ddot{\boldsymbol{r}}[\tilde{\alpha}(\lambda^{(k)}, L)] + \mu \frac{\boldsymbol{r}[\tilde{\alpha}(\lambda^{(k)}, L)]}{r[\tilde{\alpha}(\lambda^{(k)}, L)]^3} \tag{25}$$

If a mixed coast-thrust or thrust-coast arc is required, an additional design parameter ε representing the switching time is introduced. For example, if a thrust-coast arc is considered, the arrival conditions at the kth planet, as in Eq. (23), are used to analytically back propagate the trajectory up to the switching time, and then a thrust arc is computed with the inverse method, taking the outgoing conditions from the kth flyby, and the absolute position and velocity at the switching point.

For each transfer arc, the sequence of thrust-coast arcs has to be decided a priori, based on experience. Four possible switching strategies have been implemented: all thrust, all coast, thrust-coast, and coast-thrust. The first one is generally used for spirals when no additional information is available. The last two can be used when a maneuver is required at the beginning or at the end of the transfer leg, respectively, whereas the second one is for purely ballistic arcs.

III. Problem Formulation

The preliminary design of a general low-thrust, multiple gravity-assist trajectory is formulated as a global optimization problem of the form

$$\min F(\boldsymbol{y}) \tag{26}$$

subject to

$$\boldsymbol{h}(\boldsymbol{y}) = \boldsymbol{0}, \qquad \boldsymbol{g}(\boldsymbol{y}) \leq \boldsymbol{0} \tag{27}$$

with $\boldsymbol{y} = [z, \boldsymbol{y}_r]$, $\boldsymbol{y}_r \in D_r \subseteq \Re^n$, and $z \in D_i \subseteq Z$, where D_r and D_i are, respectively, the solution domains containing the real part and the integer part of the solution vector $\boldsymbol{y}$, defined as

$$\begin{aligned}\boldsymbol{y} = [&n_R^{(1)}, \ldots, n_R^{(k)}, \ldots, n_R^{(N_p-1)}, v_\infty^E, \psi, \theta, \boldsymbol{v}_{\text{in}}^{(1)}, \ldots, \boldsymbol{v}_{\text{in}}^{(k)},\\ &\ldots, \boldsymbol{v}_{\text{in}}^{(N_p-1)}, t_1, \ldots, t_j, \ldots, t_{N_p}, \boldsymbol{\lambda}^{(1)}, \ldots, \boldsymbol{\lambda}^{(k)}, \ldots,\\ &\boldsymbol{\lambda}^{(N_p-1)}, r_p^{(1)}, \ldots, r_p^{(k)}, \ldots, r_p^{(N_p-2)}, \ldots, \eta^{(1)}, \ldots, \eta^{(k)},\\ &\ldots, \eta^{(N_P-2)}, \varepsilon^{(1)}, \ldots, \varepsilon^{(k)}, \ldots, \varepsilon^{(N_P-2)}]^T\end{aligned} \tag{28}$$

where $n_R^{(k)}$ is the integer defining the number of revolutions around the sun for each phase k, $r_p^{(k)}$ is the pericenter radius for each flyby divided by the planet mean radius, and $\eta^{(k)}$ represents an auxiliary angle used to identify the plane of the swingby hyperbola [39].

Constraints on the maximum level of thrust and terminal time are defined by

$$g_k = |\boldsymbol{u}^{(k)}| \leq u_{\max}^{(k)}, \qquad k = 1, \ldots, N_p - 1 \tag{29}$$

$$h_k(\boldsymbol{y}) = T^{(k)}(\boldsymbol{y}) - (t_j - t_{j-1}) = 0, \qquad j = 2, \ldots, N_p \tag{30}$$

The mixed integer–nonlinear programming problem in Eqs. (26) and (27) is, in general, not structured, highly nonlinear, not differentiable, and discontinuous [40]. Different studies have empirically proven that problems with such characteristics can be effectively approached with stochastic optimization methods and, in particular, with evolutionary algorithms that have proven to perform satisfactorily in these cases [41]. Because evolutionary algorithms generally solve box-constrained problems, Eqs. (26), (29), and (30) would be typically reformulated through an indirect solution method with static penalty parameters, and a measurement of the constraints violation:

$$f_p(\boldsymbol{y}) = c_1 F(\boldsymbol{y}) + c_2 \sum_{k=1}^{N_P-1} |h_k(\boldsymbol{y})| + c_3 \sum_{k=1}^{N_P-1} \langle g_k(\boldsymbol{y}) \rangle \tag{31}$$

with

$$F(\boldsymbol{y}) = \sum_{k=1}^{N_p-1} m_r^{(k)} \tag{32}$$

where $m_r^{(k)}$ is the ratio between the propellant mass and the total mass, relative to phase k. Constraints are then normalized to evaluate the relative violation:

$$\hat{h}_k(\boldsymbol{y}) = \frac{T^{(k)}(\boldsymbol{y}) - (t_j - t_{j-1})}{(t_j - t_{j-1})} = 0 \tag{33}$$

$$\hat{g}_k(\boldsymbol{y}) = \frac{(\max |\boldsymbol{u}^{(k)}|) - u_{\max}^{(k)}}{u_{\max}^{(k)}} \leq 0 \tag{34}$$

thus, the augmented objective function in Eq. (31) is finally defined as

$$f_p(\boldsymbol{y}) = c_1 \sum_{k=1}^{N_p-1} |\hat{h}_k(\boldsymbol{y})| + c_2 \sum_{k=1}^{N_p-1} \langle \hat{g}_k(\boldsymbol{y}) \rangle + c_3 F(\boldsymbol{y}) \tag{35}$$

Constants c_1, c_2, and c_3 would be empirically tuned to converge to a set of feasible solutions satisfying firstly the time constraint, which represents a physical constraint, and secondly the thrust constraints, which are related to technological limits. However, because the global optimization technique employed in this work is devised to handle inequality constraints directly, a more effective approach has been adopted. The constraint on the time of flight has been explicitly solved by translating it into an inequality constraint that requires the actual time of flight given in Eq. (30) to have a maximum 2% difference with respect to the required T, and the constraint on the maximum acceleration attainable has been weighted into the objective function with a penalty term. This approach has proven to be the best compromise for the effective solution of the constrained problem. In fact, the time constraint has a high priority in the design process, because it represents a physical constraint, whereas the thrust constraint, which is a technological limit, has a secondary importance in the solution of a preliminary design problem. Moreover, it has been observed that if the two constraints are either treated explicitly or both weighted in the augmented objective function, the satisfaction of the time constraint plays against the satisfaction of the thrust constraint. For this reason, the two constraints are treated differently. In this way, at first, solutions that are physically meaningful are found, and then among the feasible solutions, the propellant mass ratio is optimized while satisfying the maximum acceleration available. This method reduces the number of penalty weights that must be introduced in the objective function and has proven to ease, at the same time, both the satisfaction of the thrust constraint and the minimization of the propellant.

It has to be noticed that, although the proposed shape-based method does not generally provide an optimal solution according to optimal control theory, it always yields feasible trajectories for a

given level of thrust or other orbital characteristics such as departure and arrival velocities, time of flight, or a particular sequence of planets. On the other hand, all of the solutions presented in the following section are locally optimal with respect to the problem in Eq. (26) and (27). It is nevertheless expected that as the shape of the pseudoelements approaches the solution of the corresponding optimal control problem, the inverse method will yield the associated optimal control for the thrust.

The possibility of simultaneously enforcing the desired values on position and velocity at the boundaries, on thrust level, and on time of flight distinguishes the pseudoequinoctial method from the exponential-sinusoid approach proposed by Petropoulos et al. [35]. This higher flexibility is paid with a higher number of free parameters that have to be set during the optimization process, though their value has a much clearer physical meaning because they are directly related to orbital parameters. As an example, looking at Fig. 2b, a high value of the shaping parameter for the exponential shape of the semilatus rectum causes a rapid increase of the parameter at the beginning of the orbit and a slow increase at the end, which corresponds to a high thrust level at the beginning and a low thrust level at the end.

IV. Global Search Through a Hybrid Evolutionary Algorithm

The global optimization problem formulated in the previous section has been solved using a novel evolutionary algorithm based on a hybridization of a branching and an evolutionary step. A discussion about the performances of the algorithms is beyond the scope of this paper and has already been developed in other works [38,42]. In the following discussion, only a brief reminder of the basic working principles of the algorithm will be presented to better understand the results obtained in this paper. The discussion will focus, in particular, on the treatment of the inequality constraints.

The proposed optimization approach, implemented in a software code called EPIC, is based on evolutionary branching (EB) [38]. Evolutionary branching is a hybrid deterministic-stochastic approach to the solution and characterization of constrained and unconstrained multimodal, multivariate, nonlinear programming problems with mixed integer–real variables and discontinuous quantities. The EB approach is based on the following principal ideas:

An evolutionary algorithm is used to explore the solution space $D = D_r \cup D_i$. Then a branching scheme, dependent on the findings of the evolutionary step, is used to partition the solution domain into subdomains. On each subdomain, a new evolutionary search is performed. The process continues until a number of good minima and, eventually, the global one are found. Nonpromising subdomains are instead pruned out.

The search is performed by a number of individuals (explorers): each solution $\boldsymbol{y}$ is associated to an individual and is represented by a string of length n, containing, in the first s components, integer values and in the remaining n-s components, real values. A hypercube S enclosing a region of the solution space surrounding each individual is then associated to $\boldsymbol{y}$. In analogy with neighborhood search techniques, the solution space is explored locally by each explorer, acquiring information about the landscape within the associated region S and globally randomly sampling D by a mutation of the worst individuals in the population.

At every generation, all of the individuals showing some improvement communicate their findings to the others, in order to evolve the entire population toward a better status. During the evolutionary step, a discoveries–resources balance is maintained: a level of resources is associated to each individual and is reduced or increased depending on the number of good findings of the individual.

A. Constraint-Handling Technique

At each evolution step, the population of solutions is divided into two subpopulations and a different objective function is assigned to each one; namely, one subpopulation aims at minimizing the original objective function, whereas the other aims at minimizing the residual on the constraints defined as

$$\min_{y \in D} f = \sum_{j=1}^{m} \max([0, R_j]) \tag{36}$$

where m is the number of violated constraints and R_j is the residual on the jth violated constraints. The two subpopulations are coevolved in parallel, and individuals are allowed to move from one population to the other. Moreover, if f^* is the value of the fitness function of an individual $\boldsymbol{y}$ inside the feasible set, the fitness function of a new individual, or a sample, generated from $\boldsymbol{y}$, is augmented in the following way:

$$\min_{y \in D} f = \begin{cases} f^* & \text{if every } R_j \leq 0 \\ f^* & + \max \mathbf{R} \text{ if any } R_j > 0 \end{cases} \tag{37}$$

The strategy of coevolving two populations with the two different goals described previously allows a flexible search for feasible optimal solutions: either all feasible solutions are forced to remain feasible or just a subset of them are forced to preserve feasibility and the others are allowed to become infeasible. In the latter case, the result is a more extensive search along the boundary of the feasible region, while preserving the feasibility of at least the best solution. This is particularly desirable in the case of nested minima along the boundaries of the feasible region.

B. Stopping Criteria

In this work, three stopping criteria are used: the maximum number of function evaluations, the number of subdomains, and the convergence of the best individual (only for the evolutionary step). All of them are based on some heuristics and not on any rigorous proof of global convergence. It should be noted, however, that the branching scheme is devised to asymptotically partition the whole domain D into infinitesimal subdomains and therefore to converge globally. Finally, solution accuracy is enhanced by starting a local search with a sequential quadratic programming (SQP) algorithm from each one of the best solutions found by the evolutionary-branching algorithm.

V. Test Cases

The methodology presented in the previous sections is the core of a preliminary design tool, implemented in MATLAB, called Interplanetary Mission Analysis Global Optimization (IMAGO). In the following discussion, a number of transfer trajectories of increasing complexity are used to test IMAGO.

IMAGO is made up of two modules: a trajectory-model generating module and a global search engine. The first module computes the value of the augmented objective function in Eq. (35) and of the constraints in Eqs. (33) and (34) according to the shape-based model described in Sec. II. In this implementation, EPIC is used as the search engine to find a solution to the problem in Eqs. (26) and (27). EPIC takes the value of the $f_p(\boldsymbol{y})$ as an input and associates the solution vector in Eq. (28) to an individual. The parameters forming $\boldsymbol{y}$ are then modified (according to the EB paradigm) during the optimization process till the stopping criteria in EPIC are satisfied. Notice that a general nonlinear programming solver can be used instead of EPIC to find a locally optimal solution.

First, a low-thrust transfer to Mars is presented, together with the main features of the adopted shape, followed by a rendezvous transfer to Mercury. Then a flyby mission to Mercury with a Venus swingby is investigated and, finally, different options for Jupiter are presented. All of the test cases have been performed on an Intel Pentium 4 1.7 GHz with Windows XP.

A. Low-Thrust Transfer to Mars

The aim of this test is to analyze and compare the characteristics of the linear and exponential shapes and to assess the effectiveness of

Table 1 Comparison between the linear-trigonometric and the exponential shape

Shaping method	Solution number	Launch date, MM-DD-YY	TOF, day	Prop. mass ratio
Linear-trigonometric shape	1	21 May 2028	813	0.177
	2	15 May 2030	998	0.188
Exponential shape	1	25 May 2028	717	0.179
	2	05 May 2028	805	0.179

the proposed approach at the preliminary design of direct transfers. Both shapes have been used to design low-thrust trajectories to Mars in the range of launch dates from 2028 to 2031, with zero departure and arrival velocities. No coast arcs are introduced, because the interest of this test is to purely analyze the behavior of the two shaping functions when they are used to model a continuous low-thrust spiral. The acceleration is constrained to be below $1.5 * 10^{-4}$ m/s^2, and the time of flight can vary between 600 and 1000 days, thus offering a wide range of possible transfer options. All shaping parameters $\boldsymbol{\lambda}$ belong to the interval $[-0.5, 0.5]$ for the exponential shape, whereas for the linear-trigonometric shape, the shaping parameter λ_1 for the semilatus rectum belongs to the interval $[-0.5, 0.5]$, and the other two shaping parameters λ_2 and λ_3 belong, respectively, to the intervals $[-0.1, 0.1]$ and $[-0.01, 0.01]$. The specific impulse for this case has been set to 3000 s, and the solution vector is $\boldsymbol{y} = [n_R, t_1, t_2, \lambda_1, \lambda_2, \lambda_3]^T$, that is, the number of revolutions, the initial and transfer time, and the three shaping parameters; in this case, the launch and arrival velocities are set to zero.

Table 1 shows the first two solutions found for each shape at the end of two independent runs, one for each shape. Only the evolutionary part of EPIC was used, setting a population of 20 individuals, of which only 12 were forced to be feasible. The resulting computational time for each run was about 10 min. The obtained 12 feasible solutions were located around the optimal launch dates and were different in the transfer time and the propellant consumption. Solution 1 for the linear-trigonometric shape has been plotted in Fig. 3a, and solution 1 for the exponential shape has been plotted in Fig. 3b; for both plots, the arrows represent the thrust direction, and the length is proportional to the magnitude of the thrust. It can be noted that both shapes locate the same launch windows and produce very similar estimates of the propellant mass consumption, however, each shape yielded different characteristics of the transfer.

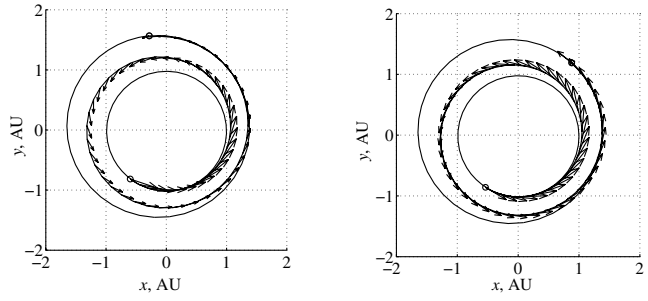

Fig. 3 Earth–Mars transfer arrows represent the thrust vector: a) linear-trigonometric shape and b) exponential shape.

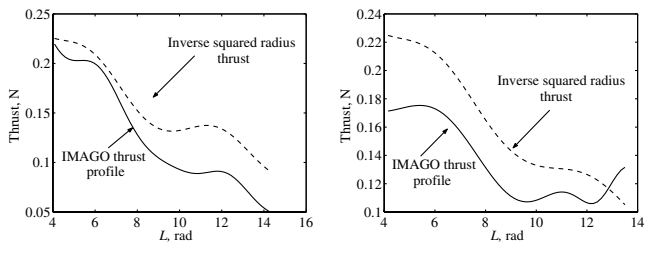

Fig. 4 Acceleration profile: a) linear-trigonometric shape and b) exponential shape.

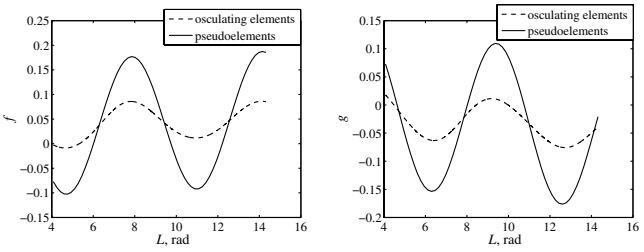

Fig. 5 Linear-trigonometric shape, comparison for: a) *f* element and b) *g* element.

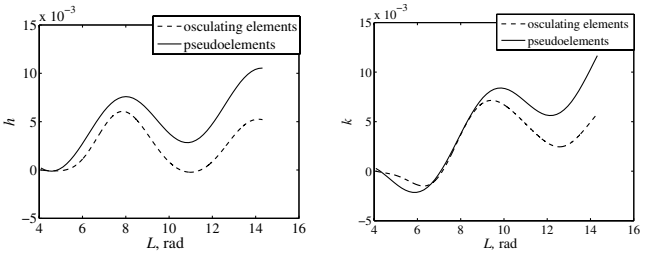

Fig. 6 Linear-trigonometric shape, comparison for: a) *h* element and b) *k* element.

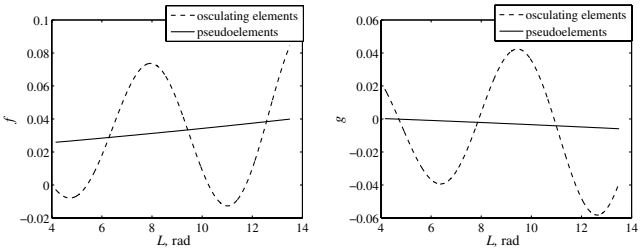

Fig. 7 Exponential shape comparison for: a) *f* element and b) *g* element.

In Figs. 4a and 4b, the actual thrust acting on the spacecraft, which has been assumed to have an initial mass after launch of 1535 kg, has been compared with a reference thrust with a maximum value of 220 mN at 1 AU and which is decreasing with the inverse of the squared of the distance from the sun. Figure 4a shows how the linear-trigonometric shape produces a control acceleration profile that quite closely follows the reference profile.

As a further validation, a comparison has been performed between the pseudoequinoctial elements and the propagated elements subject to the control found by IMAGO. As can be seen in Figs. 5 and 6, the propagated osculating elements and the pseudoelements obtained with the linear-trigonometric shape have the same frequency and the same secular component. On the other hand, Figs. 7 and 8 show how the exponential shape correctly reproduces the mean behavior of the osculating elements. In both cases, the osculating element p is closely reproduced by the shaped elements (see Fig. 9). In addition, if the comparison is done in terms of the Cartesian state vector, it can be

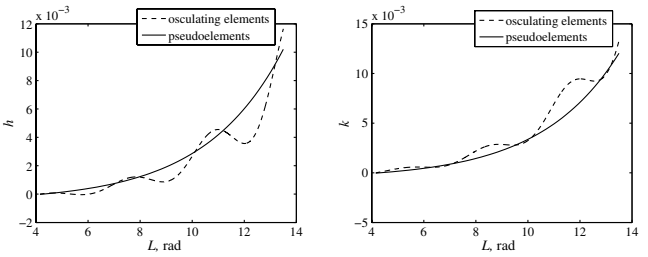

a) b)

Fig. 8 Exponential shape comparison for: a) h element and b) k element.

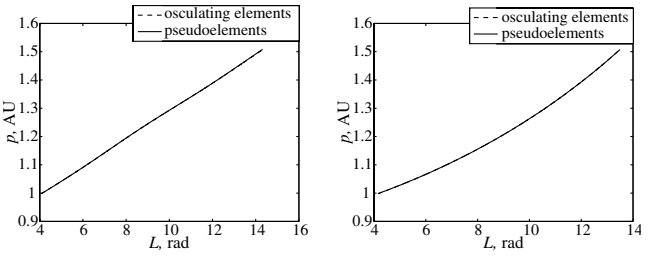

a) b)

Fig. 9 Comparison for element p: a) linear-trigonometric shape and b) exponential shape.

found that the shaped trajectory very closely matches the propagated trajectory. The discrepancy between the two is due to the neglected terms in $\mathrm{d}L/\mathrm{d}t$. The resulting maximum relative error was of the order of 10^{-5} in position and 10^{-4} in velocity.

Several numerical tests have demonstrated that, on average, the exponential shape presents a more flexible behavior with respect to the linear-trigonometric one. In fact, for this test case, the exponential shape provided a larger range of feasible transfer options with times of flight ranging from 600 to 1000 days. In addition, the obtained solutions were characterized by a large variety of control profiles, such as quasiconstant, decreasing, and even increasing. Because the main difference between the two shapes is represented by the secular term (linear or exponential), the results for the acceleration profile suggest that a polynomial secular term with a variable exponent could properly represent both solar and nuclear electric propulsion. This alternative shape is already under study and will be presented in future papers.

B. Low-Thrust Transfer to Mercury

Mercury, due to the eccentricity and high inclination of its orbit, is a challenging target requiring high energy changes. A direct transfer to Mercury would test the ability of the proposed shaping method to deal with multiple revolution trajectories in 3-D. Launch and arrival relative velocities are set to zero, the maximum acceleration is constrained to $5 * 10^{-4}$ m/s^2, the $I_{\mathrm{sp}} = 3200$ s, and the maximum time of flight is 1400 days. For this test, the exponential shape has been used and the three shaping factors have been bounded to be $\boldsymbol{\lambda} \in [-0.1, 0.1]$. EPIC has then been applied to this case, employing a population of 40 individuals, of which 10 were forced to be feasible, with two levels of branching, and a maximum number of 20

Table 2 Comparison between IMAGO solution and DITAN optimized solution

Solver	Launch date, MM-DD-YY	TOF, day	Prop. mass ratio
IMAGO	25 Feb. 2014	1110	0.535
DITAN	18 Apr. 2014	1084	0.515

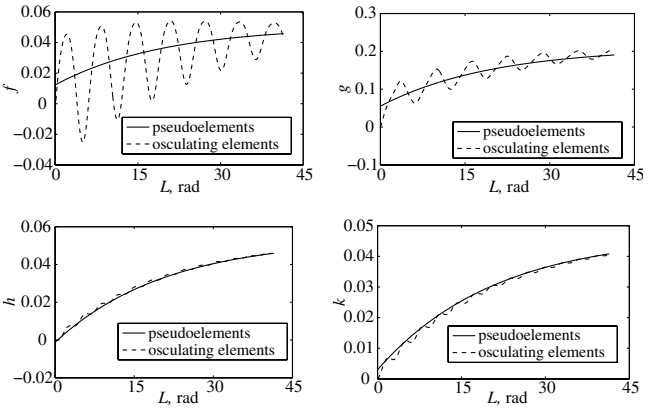

Fig. 10 Shaped and osculating elements for the Earth–Mercury transfer.

subdomains. The departure date was bound to be within the interval $t_0 = [3285, 5475]$ [modified Julian date (MJD2000), starting 1_January_2000, 1200 hrs] and the number of revolutions within the interval $n_R = [1, 6]$. For this test, the computational time was about 3 h and the number of optimization parameters $\boldsymbol{y} = [n_R, t_1, t_2, \lambda_1, \lambda_2, \lambda_3]^T$ is the same as in the case of Mars. It can be noticed that the computational time is not only dependent on the complexity of the optimization problem, but also by the depth of the search (i.e., branching levels).

The optimizer found over 200 feasible solutions completely describing the structure of the launch window. Among them, the osculating equinoctial parameters of one of the best ones were plotted in Fig. 10 and compared with the shaped parameters. As can be seen, the shaped parameters follow the mean value of the osculating parameters.

The in-orbit plane (elevation) and out-of-orbit plane (azimuth) components of the thrust have been plotted in Fig. 11a. The elevation is defined as the angle between the velocity vector and the projection of the thrust vector onto the plane of the osculating orbit, therefore a thrust vector aligned with the velocity vector would have zero elevation. The azimuth is the angle between the thrust vector and its projection onto the osculating orbital plane, therefore an azimuth of 90 deg corresponds to a thrust vector perpendicular to the orbital plane in the direction of the angular momentum. It is remarkable how the out-of-plane component, which oscillates once per orbit, reaches its maximum amplitude when the spacecraft is far from the sun. Figure 11b shows how the thrust always remains below the imposed constraint; it is also interesting to notice how the thrust profile, although not being an optimal control solution, is similar to the switching structure that the optimal control would yield. As a further validation of the result, the solution obtained with IMAGO was used as a first guess for a refined optimization with the software for direct interplanetary trajectory analysis (DITAN) that implements a direct-collocation method by direct finite elements transcription (DFET) [22]. Here and in the following test cases, the departure dates, transfer times, swingby altitudes, incoming conditions, and maximum thrust levels provided by IMAGO have been used as first-guess values to

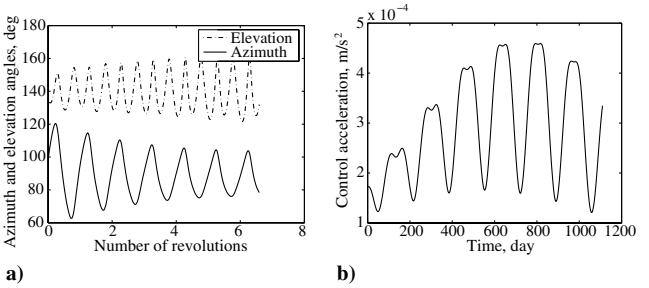

a) b)

Fig. 11 Earth–Mercury transfer: a) azimuth and elevation thrust angles and b) control acceleration profile.

start an optimization with DITAN. In this implementation, however, neither the control profile nor the evolution of the Cartesian parameters have been used to initialize the value of the collocation points for the DFET transcription. Nevertheless, all of the first-guess solutions generated by IMAGO converged to local optimal and feasible solutions for DITAN.

Notice that even in this case no coast arc was explicitly introduced in the shape-based model because, as in the previous case, only the way the shaping function was modeling a long low-thrust spiral was of interest. On the other hand, the obtained result suggests that, even without imposing any switching structure (sequence of coast and thrust arcs), the shaping method was able to reveal the underlying structure. The gain in the objective function due to an optimal switching structure can be read in the result yielded by DITAN, which, starting from the solution computed with IMAGO, automatically generated a locally optimal solution with an optimal sequence of coast and thrust arcs.

As can be read in Table 2 the two results are in good agreement. Notice that the first guess produced by IMAGO overestimates the minimum required propellant. This was expected, however, because the control law defined by IMAGO is not, as explained previously, an optimal control law.

C. Low-Thrust Transfer to Mercury via a Venus Swingby

The purpose of this third test case is twofold: one, to test the capability of the tool at treating 3-D transfers exploiting the beneficial combination of low-thrust propulsion and gravity-assist maneuvers in order to reach a high inclination target, and two, to compare the proposed approach to a similar analysis performed with STOUR-LTGA [36,37]. The problem is to transfer a spacecraft to Mercury via a Venus swingby in the year 2002. Table 3 shows the bounds used for the search performed by IMAGO with a population of 40 individuals, 20 of which were forced to reach feasibility. For this case, the total number of optimization variables was equal to 18, and the solution vector was described by

$$\boldsymbol{y} = [n_R^{(1)}, n_R^{(2)}, v_\infty, \varphi, \vartheta, t_1, t_2, t_3, \lambda_1^{(1)}, \lambda_2^{(1)}, \lambda_3^{(1)}, \lambda_1^{(2)}, \lambda_2^{(2)}, \lambda_3^{(2)}, \boldsymbol{v}_{\text{in}}^{(1)}, \boldsymbol{v}_{\text{in}}^{(2)}, r_p, \eta]^T$$

The linear-trigonometric shape was adopted for this test because it can reproduce the profile of a SEP engine, and the shaping parameters have been bounded to be $\boldsymbol{\lambda} \in [-0.5, 0.5]$. The first guess produced by IMAGO, with a computational time of about 40 min was compared, at first, with the solution found by STOUR-LTGA and then was used to initialize the software DITAN.

Table 3 Bounds on the Earth–Venus–Mercury transfer

Parameter	Value
Launch year	2002
Escape velocity, km/s	3
Earth–Venus TOF (day)	[100–220]
Max Acc. Earth–Venus, m/s^2	$1.5 * 10^{-4}$
I_{sp}, s	3000
Max number of revolutions, Earth–Venus leg	2
Minimum flyby altitude, km	300
Venus–Mercury TOF, day	[500–1000]
Max Acc. Venus–Mercury, m/s^2	3e-4
Max number of revolutions, Venus–Mercury leg	7
Max arrival velocity, km/s	5

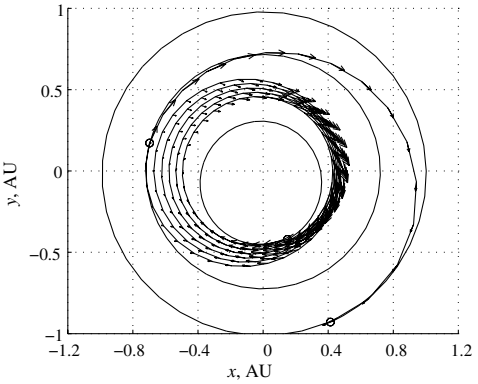

Fig. 12 Earth–Venus–Mercury transfer, arrows represent the thrust vector.

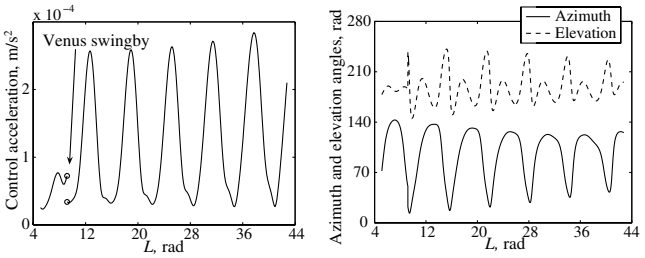

a) **b)**

Fig. 13 Earth–Venus–Mercury transfer: a) control acceleration profile and b) azimuth and elevation angles.

As can be seen in Table 4, the solution found by IMAGO is in good agreement with the result of STOUR-LTGA, both in terms of launch date and time of flight. Moreover, it has to be underlined that the first-guess solution provided by IMAGO is very close to the optimized one optimized with DITAN. Even in this case, all of the first-guess solutions provided by IMAGO converged to local optimal solutions for DITAN, with a lower propellant consumption.

Both Fig. 12, in which the trajectory is projected onto the ecliptic plane along with the control thrust vector, and Fig. 13a show how the thrust is quite low at the aphelion, whereas it has its maximum value at the perihelion where, of course, the propulsion is more effective. This is a further confirmation of the correct transcription of the solution, because the theoretical optimal control solution would have a bang-bang structure with no thrust at the aphelion and maximum thrust at the perihelion. This also gives an explanation of the overestimation for the propellant consumption, because the adopted inverse model is not capable of switching off the engine, thus resulting in an excessive propellant consumption. Finally, it can be noticed how the required thrust level increases toward Mercury, correctly reproducing the effect of an increasing solar flux.

Figure 13b shows the azimuth and elevation angles of the thrust vector. Even in this case, the maximum amplitude of the oscillation of the azimuth angle occurs far from the sun, although less evident than in the previous case. On the other hand, unlike the previous case, the in-plane component of the thrust oscillates around 180 deg.

D. Low-Thrust Transfer to Jupiter

In a previous work [39] it was shown how IMAGO could be effectively used for the investigation of the best sequences to reach a

Table 4 Summarizing and comparison of Earth–Venus–Mercury transfer

Solution method	Launch date, MM-DD-YY	v_∞, km/s	Venus–Earth TOF, day	Flyby altitude, km	Venus–Mercury TOF, day	Total TOF, day	Prop. mass ratio
STOUR-LTGA	02 Aug. 2002	3	184	N.A.	687	851	0.526
IMAGO	16 Jul. 2002	3	186	201	746	932	0.220
DITAN	11 Jul. 2002	3	186	300	770	956	0.185

Table 5 Solution domain for the Earth–Mars–Mars–Jupiter option

Bounds	t_0, MJD2000	T_1, day	r_{p1}	T_2, day	ε_1	r_{p2}	T_3, day	v_∞, km/s
U_b	3500	200	1	600	0	1	1400	1
L_b	4380	330	15	750	0.7	15	2000	5

Table 6 Summary of different options for the double Mars swingby transfer to Jupiter

Solution	Launch date, MM-DD-YY	C_3, km^2/s^2	TOF, day	Arrival v_∞, km/s	Prop. mass ratio
EMMJ-1	Nov. 21, 2011	10.9	2664	3.66	0.29
EMMJ-2	Oct. 13, 2009	10.7	2909	3.91	0.27
EMMJ-3	Oct. 9, 2009	10.7	2915	3.92	0.23

given target through a ballistic multiple gravity-assist (MGA) trajectory. It was also argued that optimal ballistic MGA solutions could be extremely useful even for LTGA trajectories. For example, it was shown that in the case of a transfer to Jupiter, besides the typical pure ballistic options exploiting multiple swingbys of the inner planets, there could be some interesting transfer opportunities that present low departure and arrival velocities at the cost of a relevant deep-space maneuver (typically larger than $1 - 1.5$ km/s). This was the case for the sequence EMMJ, found in the aforementioned work, which presented a reduced departure and arrival velocity, at the cost of a corrective maneuver after Mars greater than 2 km/s.

The same solution can now be optimized using low-thrust propulsion to achieve the required Δv in a more efficient way. A thrust arc is inserted between the last swingby planet and Jupiter, setting the maximum thrust-to-mass ratio to $1.7 * 10^{-4}$ m/s^2 with a specific impulse of $I_{sp} = 3000$ s. The shape used for the description of the thrust arc is the linear-trigonometric, and the shaping parameter $\boldsymbol{\lambda}$ has been bounded within the set $\boldsymbol{\lambda} \in [-0.1, 0.1; \quad -0.1, 0.1; \quad -0.01, 0.01]$, with a reduced interval for the out-of-plane pseudoelements, because the out-of-plane motion is expected to be less significant. A population of 40 individuals was used with 20 individuals forced to be feasible.

The solution vector is

$$\boldsymbol{y} = [n_R^{(3)}, v_\infty, \varphi, \vartheta, t_1, t_2, t_3, t_4, \lambda_1^{(3)}, \lambda_2^{(3)}, \lambda_3^{(3)}, \boldsymbol{v}_{\text{in}}^{(3)}, r_p^{(1)}, r_p^{(2)}, \eta_p^{(1)}, \eta_p^{(2)}, \varepsilon^{(1)}]^T$$

and the problem dimension is 17. In this case, phases 1 and 2 are described by coast arcs and deep-space maneuvers, and phase 3 contains a multirevolution low-thrust arc.

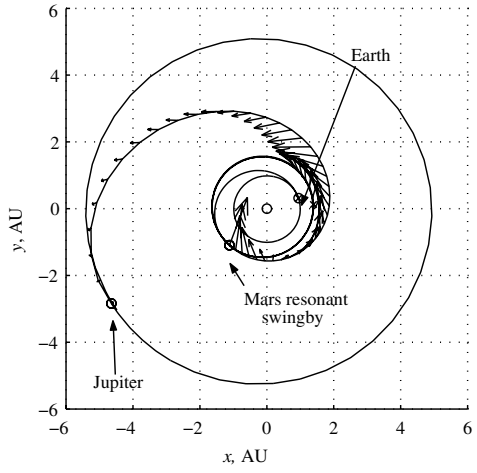

Fig. 14 Earth–Mars–Mars–Jupiter transfer, arrows represent the thrust vector.

The solution domain is defined in Table 5, where the range of the launch date was obtained from the impulsive solutions. At the end of the optimization process, about 20 feasible solutions have been identified, spanned over the two optimal launch dates and typically presenting differences either in the arrival velocity, the launch dates, or the total transfer time. In Table 6, two of the most interesting solutions, obtained after 1.5 h of computational time, are reported. Solution EMMJ-1, although more expensive, has a slower arrival at Jupiter, which makes this option even more appealing, also considering the reduced time of flight. Furthermore, it is interesting to note that despite that no model for resonant orbits being introduced, the algorithm nevertheless spontaneously found a resonant orbit with Mars.

Solution EMMJ-2, plotted in Fig. 14, has been further optimized with DITAN using a realistic model for the power generated by the solar array. The optimized result, reported for comparison in the last column of Table 6, is in good agreement with the first-guess solution provided by IMAGO. In particular, the launch date and encounters with Mars have been correctly guessed and the mass ratio has been further improved.

The last test case is still a LTGA transfer to Jupiter, but with the sequence Earth–Venus–Earth–Jupiter (EVEJ), to allow a direct comparison with STOUR-LTGA [43]. The launch is foreseen in the year 2015 and a thrust-coast arc has been set after the Earth flyby. The exponential shape has been adopted, setting the shaping parameter $\boldsymbol{\lambda} \in [-0.5, 0.5]$. Transfer times for each leg have been bound to be in an interval of 200 days around the values reported for the STOUR-LTGA solution. The minimum pericenter altitude for each swingby was set to 300 km above the surface of the planet.

As can be seen in Table 7, IMAGO located an interesting solution for this transfer with a smaller arrival velocity, but with comparable propellant consumption. The solution vector, made of 32 solution parameters, was calculated with a population of 40 individuals and a computational cost of 1.8 h, which yielded 20 feasible solutions mainly differing in the launch date, the total time of flight, the propellant consumption, and the arrival velocity. Then the best one was reoptimized with DITAN. As can be seen in Table 7, the solution

Table 7 Comparison between IMAGO/DITAN and STOUR-LTGA for the Earth–Venus–Earth–Jupiter transfer

Parameter	STOUR-LTGA	IMAGO	DITAN
Launch date, MM-DD-YY	09 May 2015	14 Apr. 2015	21 Apr. 2015
Departure velocity, km/s	2.0	1.8	1.8
Earth–Venus TOF, day	119	184	177
Venus flyby altitude, km	4481	8816	2431
Venus–Earth TOF, day	345	386	439
Earth flyby altitude, km	4219	5964	300
Earth–Jupiter TOF, day	1027	901	888
Arrival v_∞, km/s	5.97	4.53	5
Total TOF, day	1491	1471	1504
Prop. mass ratio	0.485	0.48	0.18

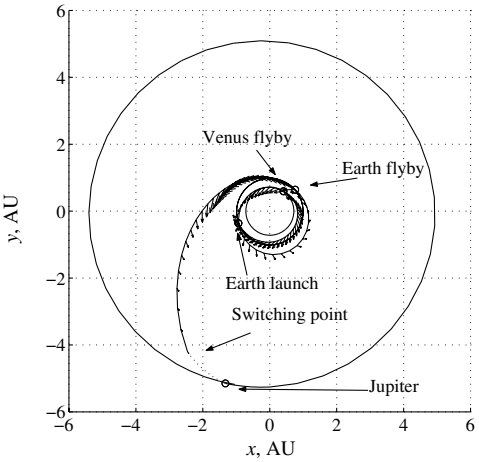

Fig. 15 Earth–Venus–Earth–Jupiter transfer, arrows represent the thrust vector.

found by IMAGO, represented in Fig. 15, and the optimized one are quite close in terms of launch dates and time of flight. This test confirms that also in the case of more complex transfers with more than one gravity-assist maneuver, the solution obtained with IMAGO is generally close, in the solution space, to a locally optimal solution for DITAN.

The main difference with respect to the optimized solution is actually the propellant mass consumption, which is overestimated as in the previous cases. Finally, it should be noticed that the number of feasible suboptimal solutions found by IMAGO increases with the dimension of the bounds on the optimization variables and with the extensive use of the branching scheme, although at the cost of a higher computational effort. For the last two cases, however, for which the goal was the analysis of an already defined impulsive solution and a comparison with STOUR-LTGA, it was not necessary to perform a search over a large interval for the design parameters.

VI. Conclusion

This paper has presented a novel approach to the preliminary design of low-thrust gravity-assist trajectories. The proposed approach combines a shape-based method with a novel global optimization algorithm and hybridizes an evolutionary-based approach and a deterministic domain decomposition technique.

Position and velocity of a spacecraft along low-thrust arcs are shaped through a parameterized set of pseudoequinoctial elements. This particular technique overcomes some of the limitations of previous shape-based approaches and allows for consistent solutions of low-thrust trajectories in three dimensions. As demonstrated in all of the test cases presented in this paper, this approach yields solutions that, though suboptimal, are sufficiently accurate for a preliminary assessment of a wide range of mission options, and are ideal, as first guesses, to initialize more accurate optimal control methods.

Two shaping functions have been presented: one made of a linear and trigonometric term that is more suitable for the description of solar electric propulsion, and a second made of an exponential function of the longitude L, which resulted in better describing nuclear electric propulsion. It can be easily proven that a constant tangential thrust (as the one provided by a NEP engine) yields a secular growth of the orbital energy that can be better represented by an exponential function. On the other hand, the linear-trigonometric shape can represent a linear secular growth of the orbital energy that corresponds to a thrust that decreases with the distance from the sun. Thus, the linear-trigonometric resulted to be more suitable for modeling a SEP engine.

Both shapes represent a compromise between accurate trajectory description and the number of shaping parameters and yield continuous control profiles that, in some cases, mimic the analogous optimal control solutions and, in general, tend to overestimate the overall mass consumption. This overestimation is a beneficial effect of the adopted model. The simplifying assumptions of a low-accuracy model could yield optimal solutions that underestimate the objective value (in the case of minimization) computed with a high-fidelity model. In this case, a designer would have a rather optimistic result with no guarantee that the mission was actually feasible.

In this paper, the preliminary solutions obtained with the proposed shape-based approach have been used to initialize a direct-collocation-based approach implementing a more sophisticated trajectory model. It is expected that the same preliminary solutions can also be used to initialize an indirect optimization method. This will provide a measure of the optimality of the shape-based solution and is, at the moment, the subject of ongoing research.

Further extensions of the proposed approach would include the definition of more flexible shapes as functions of time rather than as functions of the true longitude, thus avoiding the solution of the time constraint.

Acknowledgments

This work was started and, in part, carried out from November 2002 to April 2003, when Paolo De Pascale was a trainee in the ESA Advanced Concepts Team (ACT) at the European Space Research & Technology Center (ESTEC). He would like to thank all the members of the ACT and, particularly, Franco Ongaro.

References

[1] Rayman, D. M., Varghese, P., Lehman, D. H., and Livesay, L. L., "Results from the Deep Space 1 Technology Validation Mission," *Acta Astronautica*, Vol. 47, 2000, p. 475; also International Astronautical Congress Paper IAA-99-IAA-11.2.01, 1990.

[2] Haros, D., and Schoenmaekers, J., "Post-Launch Optimisation of the Smart 1 Low-Thrust Trajectory to the Moon," ESA Paper SP-548, Dec. 2004.

[3] Martinez-Sanchez, M., and Pollard, J. E., "Spacecraft Electric Propulsion-An Overview," *Journal of Propulsion and Power*, Vol. 14, No. 5, 1998, pp. 688–699.

[4] Williams, S. N., and Coverstone-Carroll, V., "Benefits of Solar Electric Propulsion for the Next Generation of Planetary Exploration Missions," *Journal of the Astronautical Sciences*, Vol. 45, No. 2, 1997, pp. 143–159.

[5] Sauer, C. G., Jr.,"Planetary Mission Performance for Small Solar Electric Propulsion Spacecraft," American Astronautical Society Paper AAS-93-561, 1993.

[6] Kluever, C. A., and Abu-Saymeh, M., "Mercury Mission Design Using Solar Electric Propulsion," *Journal of Spacecraft and Rockets*, Vol. 35, No. 3, 1998, pp. 411–413.

[7] Langevin, Y., "Chemical and Solar Electric Propulsion Options for a Mercury Cornerstone Mission," *Acta Astronautica*, Vol. 47, No. 2, 2000, pp. 443–452.

[8] Campagnola, S., Garcia, D., Jehn, R., Corral, C., and Croon, M., "BepiColombo Mercury Cornerstone Mission Analysis: Soyuz/Fregat Launch in 2012," ESA/European Space Operations Centre, Mission Analysis Office, Working Paper 466, Germany, Sep. 2004.

[9] Oleson, S., "Electric Propulsion for Project Prometheus," AIAA Paper 2003-5279, 2003.

[10] Yam, C., McConaghy, T., Chen, K., and Longuski, J., "Preliminary Design of Nuclear Electric Propulsion Missions to the Outer Planets," AIAA Paper 2004-5393, 2004..

[11] Vasile, M., Campagnola, S., and Bernelli-Zazzera, F., "Electric Propulsion Options for a Probe to Europa," *2nd International Symposium on Low Thrust Trajectories (Lotus 2)* [CD-ROM], Centre National d'Etudes Spatiales, Toulouse, France, 2002.

[12] Vasile, M., and Bernelli-Zazzera, F., "Targeting a Heliocentric Orbit Combining Low-Thrust Propulsion and Gravity-Assist Manuevers," *Operational Research in Space and Air* Vol. 79, Book Series in Applied Optimization, Kluwer Academic, Norwell, MA, 2003.

[13] Battin, R., *An Introduction to the Mathematics and Methods of Astrodynamics*, 1st ed., AIAA, New York, 1987.

[14] Gill, E., Murray, W., and Wright, M. H., *Practical Optimization*, Academic Press, London, 1981.

[15] Bryson, A. E., Jr., and Ho, Y. C., *Applied Optimal Control*, Blaisdell, Waltham, MA, 1969.

[16] Betts, J. T., "Survey of Numerical Methods for Trajectory Optimization," *Journal of Guidance, Control, and Dynamics*, Vol. 21, No. 2, 1998, pp. 193–207.

[17] Kluever, C. A., "Optimal Low-Thrust Interplanetary Trajectory by Direct Method Techniques," *Journal of the Astronautical Sciences*, Vol. 45, No. 3, 1997, pp. 247–262.
[18] Betts, J. T., "Using Sparse Nonlinear Programming to Compute Low Thrust Orbit Transfer," *Journal of the Astronautical Sciences*, Vol. 41, No. 3, 1993, pp. 349–371.
[19] Bertrand, R., Bernussou, J., and Barthès, I., "Optimal Low-Thrust Interplanetary Direct Transfer," International Astronautical Federation Paper 99-A.6.01, 1999.
[20] Ranieri, C. L., and Ocampo, C. A., "Finite Burn, Roundtrip Interplanetary Trajectories with ISP Constraints and Mass Discontinuities," American Astronautical Society Paper 04-231, 2004.
[21] Tang, S., and Conway, B. A., "Optimization of Low-Thrust Interplanetary Trajectories Using Collocation and Nonlinear Programming," *Journal of Guidance, Control, and Dynamics*, Vol. 18, No. 3, 1995, pp. 599–604.
[22] Vasile, M., Bernelli-Zazzera, F., Fornasari, N., and Masarati, P., "Design of Interplanetary and Lunar Missions Combining Low Thrust and Gravity Assists," ESA/European Space Operations Centre, Study Contract No. 14126/00/D/CS, Sep. 2002.
[23] Betts, J. T., *Practical Methods for Optimal Control Using Nonlinear Programming*, Society for Industrial and Applied Mathematics, Philadelphia, 2001.
[24] Herman, A. L., and Conway, B. A., "Direct Optimization Using Collocation Based on High-Order Gauss-Lobatto Quadrature Rules," *Journal of Guidance, Control, and Dynamics*, Vol. 19, No. 3, 1996, pp. 592–599.
[25] Coverstone-Carroll, V., Hartman, C. A., Herman, A. L., and Spencer, D. B., "Optimal Spacecraft Trajectory Via Higher Order Differential Inclusions," *Spaceflight Mechanics 2004*, Univelt, San Diego, CA, 2004, pp. 377–396.
[26] Casalino, L., Colasurdo, G., and Pastrone, D., "Optimal Low-Thrust Escape Trajectories Using Gravity Assist," *Journal of Guidance, Control, and Dynamics*, Vol. 22, No. 5, 1999, pp. 637–642.
[27] Miele, A., and Wang, T., "Multiple-Subarc Sequential Gradient-Restoration Algorithm, Part 1: Algorithm Structure," *Journal of Optimization Theory and Applications*, Vol. 116, No. 1, 2003, pp. 1–17.
[28] Whiffen, G., and Sims, J. A., "Application of the SDC Optimal Control Algorithm to Low-Thrust Trajectory Optimization," American Astronautical Society Paper 01-209, 2001.
[29] Petropoulos, A. E., and Sims, J. A., "A Review of Some Exact Solutions to the Planar Equations of Motions of a Thrusting Spacecraft," *Proceedings of the 2nd International Symposium on Low-Thrust Trajectory (LoTus-2)* [CD-ROM], Centre National d'Etudes Spatiales, Toulouse, France, 2002.
[30] Markopoulos, N., "Non Keplerian Manifestations of the Keplerian Trajectory Equation, and a Theory of Orbital Motion under Continuous Thrust," American Astronautical Society Paper 95-217, 1995.
[31] Hartmann, J. W., Coverstone-Carrol, V. L., and Williams, S. N., "Optimal Interplanetary Spacecraft Trajectories via Pareto Genetic Algorithm," *Journal of the Astronautical Sciences*, Vol. 46, No. 3, 1998, pp. 267_282.
[32] Azimov, D. H., and Bishop, R. H., "Optimal Transfer Between Circular and Hyperbolic Orbits Using Analytical Maximum Thrust Arcs," American Astronautical Society Paper 02-155, 2002.
[33] Bishop, R. H., and Azimov, D. H., "New Analytical Solutions to the Fuel-Optimal Orbital Transfer Problem Using Low-Thrust Exhaust-Modulated Propulsion," American Astronautical Society Paper 00-131, 2000.
[34] Tanguay, A. R., *Space Maneuvers, Space Trajectories*, Academic Press, New York, 1960, pp. 163–199.
[35] Petropoulos, A. E., Longuski, J. M., and Vinh, N. X., "Shape-Based Analytical Representations of Low-Thrust Trajectories for Gravity-Assist Applications," American Astronautical Society Paper 99-337, 1999.
[36] Petropoulos, A. E., "A Shape-Based Algorithm for the Automated Design of Low-Thrust, Gravity-Assist Trajectories," American Astronautical Society Paper 01-147, 2001.
[37] Petropoulos, A. E., and Longuski, J. M., "Automated Design of Low-Thrust Gravity-Assist Trajectories," AIAA Paper 2000-4033, 2000.
[38] Vasile, M., Summerer, L., and DePascale, P., "Design of Earth-Mars Transfer Trajectories Using Evolution-Branching Technique," *Acta Astronautica* Vol. 56, No. 8, 2005, pp. 705–720; also, International Astronautical Congress Paper IAC-03-A.7.07.
[39] De Pascale, P., Vasile, M., and Finzi, A.,"A Tool for Preliminary Design of Low-Thrust Gravity Assist Trajectories," American Astronautical Society Paper 04-250, 2004.
[40] Bliek, C., Spellucci, P., Vicente, L. N., and Neumaier, A., Algorithms for Solving Nonlinear Constrained and Optimization Problems: The State of Art, *COCONUT Project* [online progress report], http://www.mat.univie.ac.at/~neum/glopt/coconut/StArt.html [cited Jun. 2001].
[41] Back, T., Fogel, D., and Michalewicz, Z., *Handbook of Evolutionary Computation*. Inst. of Physics Publishing, London, 1998–2000.
[42] Vasile, M., "A Global Approach to Optimal Space Trajectory Design," American Astronautical Society Paper 03-141, 2003.
[43] Debban, T. J., McConaghy, T. T., and Longuski, J. M., "Design and Optimization of Low-Thrust Gravity-Assist Trajectories to Selected Planets," AIAA Paper 2002-4729, 2002.

C. Kluever
Associate Editor